IOP Publishing and International Atomic Energy Agency Nuclear Fusion
Nucl. Fusion **49** (2009) 035003 (12pp) doi:10.1088/0029-5515/49/3/035003

3D MHD VDE and disruptions simulations of tokamaks plasmas including some ITER scenarios

R. Paccagnella[1,2], H.R. Strauss[3] and J. Breslau[4]

[1] Consorzio RFX, Associazione Euratom-ENEA sulla Fusione, Padova, Italy
[2] Consiglio Nazionale delle Ricerche (CNR), Roma, Italy
[3] Courant Institute for Mathematical Sciences, New York University, NY, USA
[4] Princeton University, Plasma Physics Laboratory, Princeton, NJ, USA

E-mail: roberto.paccagnella@igi.cnr.it

Received 20 October 2008, accepted for publication 14 January 2009
Published 18 February 2009
Online at stacks.iop.org/NF/49/035003

Abstract
Tokamaks vertical displacement events (VDEs) and disruptions simulations in toroidal geometry by means of a single fluid visco-resistive magneto-hydro-dynamic (MHD) model are presented in this paper. The plasma model is completed with the presence of a 2D wall with finite resistivity which allows the study of the relatively slowly growing magnetic perturbation, the resistive wall mode (RWM), which is, in this paper, the main drive of the disruption evolution. Amplitudes and asymmetries of the halo currents pattern at the wall are also calculated and comparisons with tokamak experimental databases and predictions for ITER are given.

PACS numbers: 52.30.Cv, 52.55.Fa, 52.65.Kj, 52.55.Tn, 52.35.Py, 52.35.Mw

(Some figures in this article are in colour only in the electronic version)

Introduction

Disruptions represent one of the main concerns for tokamak operation, especially in view of fusion reactors, or experimental test reactors, such as ITER.

Several different physical phenomena, such as density limits, high Z contamination and radiative instabilities and loss of vertical equilibrium control can lead to disruptions. A very updated review is given in [1].

Generally rapid growth of global magneto-hydro-dynamic (MHD) instabilities (either resistive or ideal) leads to so-called major disruptions in which the rapid thermal quench (in a time scale of hundreds of microseconds) precedes the current quench. Instead vertical displacement events (VDEs), or vertical instabilities, develop as a consequence of a loss of vertical equilibrium control. In these cases the current quench (in a time scale of a few to tens of milliseconds) generally precedes the thermal quench. This second branch will be the subject of our study.

One of the consequences of disruptions is the appearance in the plasma edge of halo current structures, i.e. of currents which can generally conduct current to the passive structures (walls, tails, divertor plates, etc.) surrounding the plasma. These halo structures can be easily non-symmetric in the toroidal angle and can produce dangerous non-compensated horizontal forces on the vacuum vessel [2]. In ITER these forces can be of the order of several hundred MN [1].

In this paper we model the disruptions which follow a VDE which is, as noted above, the consequence of a loss of equilibrium control. By solving with the M3D code [3], a single fluid visco-resistive MHD model in the presence of a homogeneous resistive wall surrounding the plasma region, we are able to study the relatively slow evolution of the resistive wall mode (RWM). This mode is responsible in our simulations of the non-axi-symmetric current structures which develop at the plasma edge.

The paper is organized as follows: section 1 presents the physical model and implementation details; section 2 provides the result of a linear benchmarking; section 3 provides specific applications and simulation results; finally discussion and conclusions are presented.

1. 3D MHD model and boundary conditions

The resistive MHD code M3D [3] is used in these simulations. The code represents the magnetic field in potential form to ensure that the magnetic field is divergence free. The velocity is also represented in potential form to reduce numerical

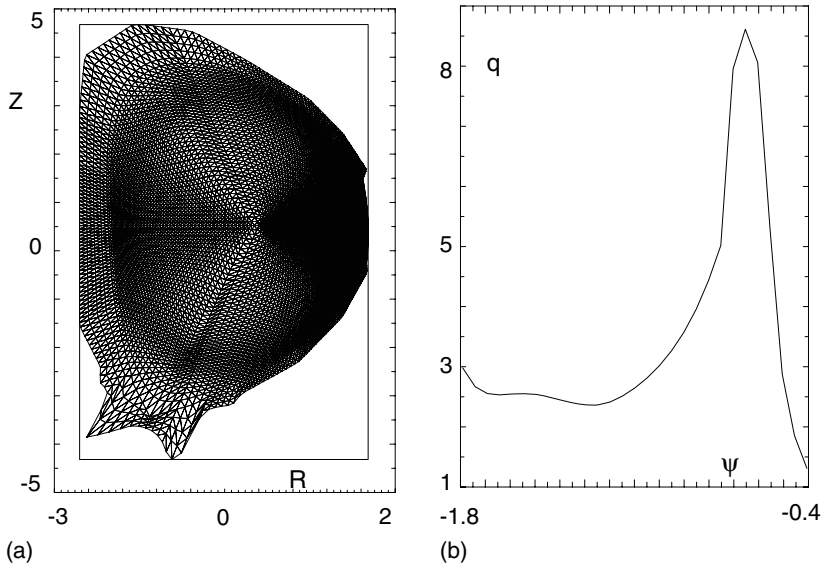

Figure 1. Initial mesh (a) and q profile (b) for the ITER-AS case.

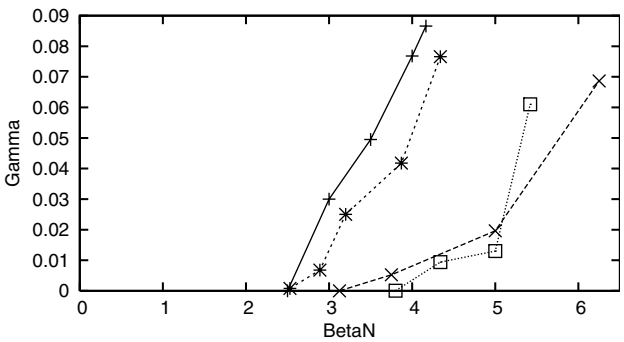

Figure 2. 'Stars' and 'crosses' are no-wall limits obtained with M3D and MARS. 'X' and 'squares' give the ideal limit for MARS and M3D.

coupling of compressional and shear Alfvén waves. The code uses a split time step. The compressional Alfvén terms and dissipative terms are solved implicitly. This allows a time step consistent with an explicit shear Alfvén wave advance, which is much larger than in a fully explicit time advance. At least two important physical parameters should be initially set by the user: viscosity and resistivity. The code uses (as is done in all the plots of this paper) normalized units: time is normalized to the Alfvèn time and length to the plasma minor radius. As regards currents, the normalized code values should be multiplied by $\mu_o B_\phi(0)/R_o$ to obtain the physical value in amperé.

The code is parallelized in two versions: an OpenMP and a massively MPI based parallelization.

The simulations reported here rely on three additional features of the code: a time dependent resistivity, an unstructured mesh and resistive wall boundary conditions. M3D has a time dependent resistivity proportional to the $-3/2$ power of the temperature, which is nearly constant along magnetic field lines. Outside the separatrix resistivity is set 10–100 times bigger than in the plasma core.

Open field lines in the halo region are in contact with the wall, which has a low temperature. Inside the magnetic separatrix, on closed field lines of the core, the temperature is high.

In three-dimensional disruption calculations, the magnetic field becomes stochastic and can no longer isolate the halo region from the core.

The regions mix and the core is cooled, resulting in a thermal quench.

M3D has a two-dimensional unstructured mesh [4] in poloidal planes.

In the toroidal direction a pseudo-spectral discretization is used.

The unstructured mesh is aligned with the magnetic field inside the magnetic separatrix, and smoothly interpolates between the separatrix and the wall. In the case of ITER modelling with both a first wall and an outer vacuum vessel, the mesh is aligned with both the first wall and the vacuum vessel.

M3D provides its own mesh generation. One option is to generate the mesh using an EQDSK file, which is a file format used by several MHD equilibrium codes. The EQDSK file contains the poloidal flux function, ψ, on a Cartesian grid. This is used to produce a mesh with sides aligned with contours of constant ψ on closed flux surfaces.

Other options include mesh generation starting from an analytically prescribed boundary. In this case the mesh is not field aligned.

MHD also has resistive wall boundary conditions [5].

The solution inside the resistive wall is matched to the exterior vacuum solution. The exterior problem is solved with Green's function method.

The vacuum field is represented as

$$B_v = \nabla\psi_v \times \nabla\phi + \nabla\lambda + I_o\nabla\phi,$$

where I_o is a constant which is equal to the constant part of I in the plasma. The reason for I_o as well as ψ_v is to be able to match the vacuum solution to a plasma equilibrium with a net current and net toroidal magnetic field. The function ψ_v depends on the poloidal coordinates R, Z and is independent

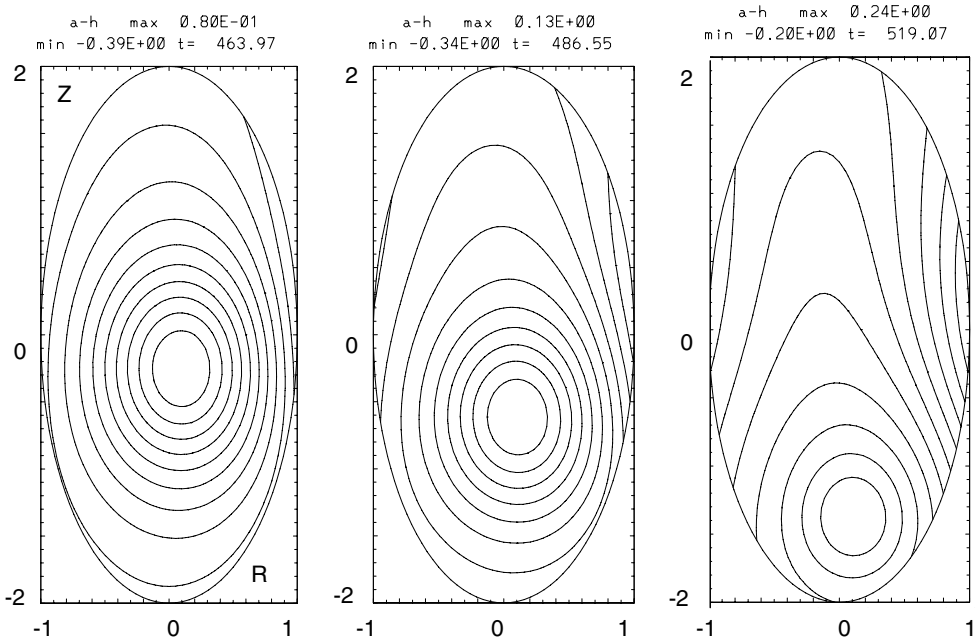

Figure 3. Poloidal flux contours time evolution for an elliptical equilibrium.

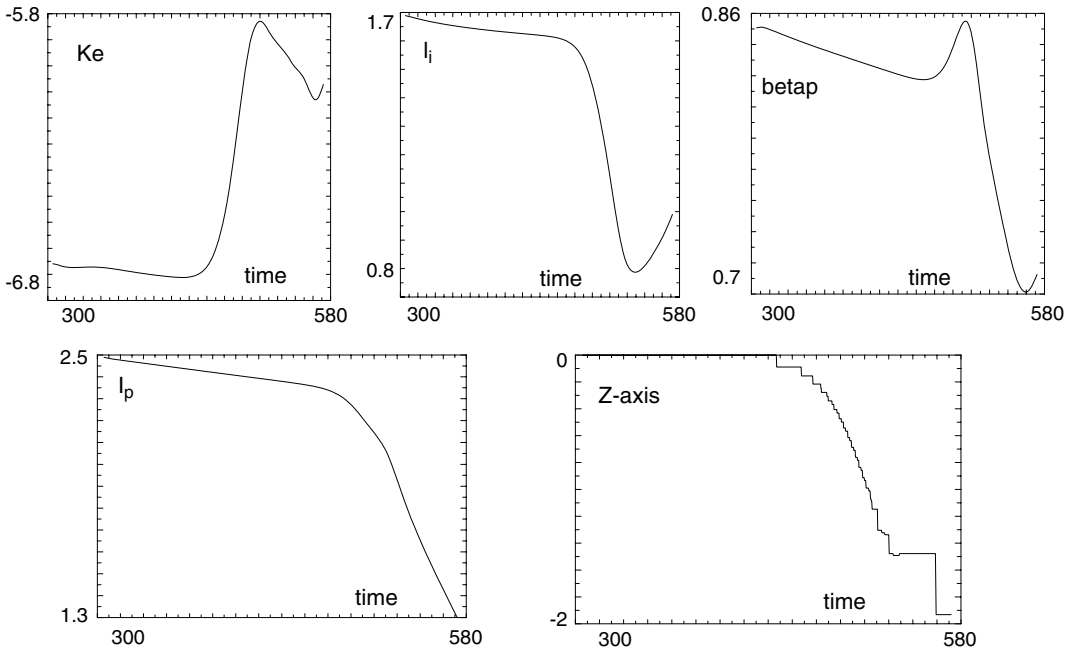

Figure 4. Time traces of kinetic energy (K_e), internal inductance (l_i), poloidal beta (betap), toroidal current (I_p) and vertical position of the magnetic axis (Z-axis).

of toroidal angle ϕ. It satisfies the vacuum Grad–Shafranov equation $\Delta^* \psi_v = 0$.

To satisfy $\nabla \cdot B_v = 0$, $\nabla^2 \lambda = 0$. On the resistive wall boundary, integrating $\nabla \cdot B$ across the thin shell gives the requirement that the normal component of magnetic field is continuous at the wall. This gives a boundary condition to determine the vacuum field.

The vacuum field is solved by the GRIN[5] code. From Green's identity one has an integral equation relating $\partial \psi_v / \partial n$ to given ψ_v and λ_n to given $\partial \lambda_n / \partial n$ on the boundary contour [6]. Here n is the normal unit vector to the boundary and $\partial / \partial n = \boldsymbol{n} \cdot \nabla$. When discretized, these integral equations become matrix equations which are set up and solved by GRIN.

Given a set of boundary points, (R_i, Z_i),

$$\left(\frac{\partial \psi_v}{\partial n} \right)_i = \sum_j K^o_{ij} \psi_{pj} + S_i,$$

$$(\lambda^n)_i = \sum_j K^n_{ij} (\boldsymbol{B}_p \cdot n)_j,$$

[5] http://w3.pppl.gov/rib/repositories/NTCC/catalog/Asset/grin.html

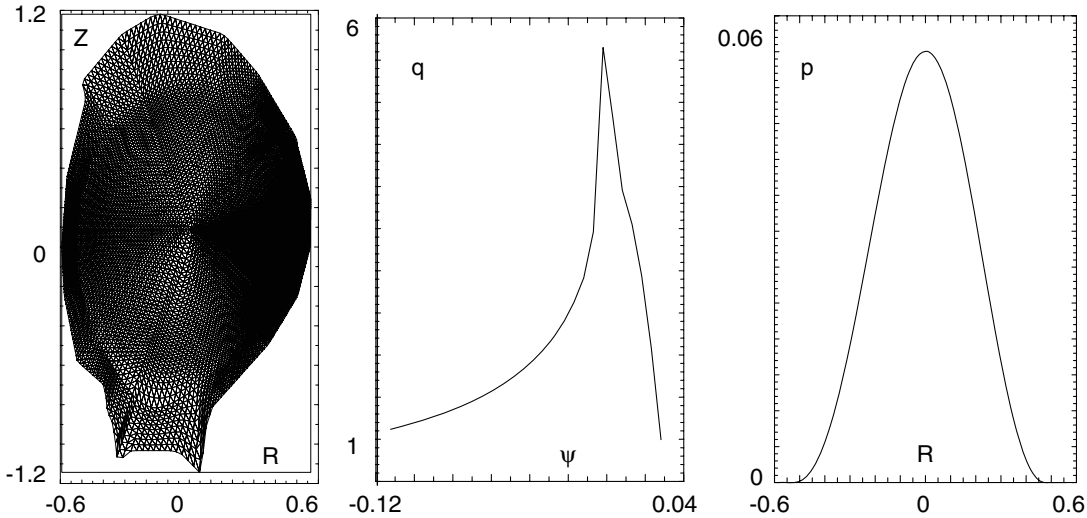

Figure 5. Mesh in the poloidal plane, q and pressure profiles.

where K^o_{ij} and K^n_{ij} are matrices that can be pre-computed given the set of boundary points.

The source term S_i can be obtained from the applied external currents or else using the 'virtual casing' method. In this method we first perform an ideal equilibrium calculation, with $\psi = 0$ on the boundary. Equating $\partial\psi_v/\partial n = \partial\psi_p/\partial n$, the source term required for equilibrium is found from $S = \partial\psi_p/\partial n$, where the right side is obtained from the ideal equilibrium.

Now the magnetic field components in the plasma have to be matched using resistive evolution at the inner boundary, which is a thin resistive shell of thickness δ and resistivity η_w. Ohm's law at the resistive wall is

$$\frac{\partial \boldsymbol{A}}{\partial t} = \nabla\Phi + \frac{\eta_w}{\delta}\boldsymbol{n} \times (\boldsymbol{B}_v - \boldsymbol{B}_p).$$

It is useful to have wall currents as a diagnostic. These have already been calculated. In the wall

$$\boldsymbol{J}^w = \nabla \times \boldsymbol{B} \approx \boldsymbol{n} \times \frac{\partial \boldsymbol{B}}{\partial n} \approx \frac{\boldsymbol{n}}{\delta} \times (\boldsymbol{B}_v - \boldsymbol{B}_p).$$

2. M3D linear benchmark with MARS for an ITER-AS scenario

Due to the complexity of the model and the novelty of the treatment of the boundary conditions it is very important to benchmark M3D with other codes, at least for the initial linear stage of the simulations. To this end we find it particularly useful to implement the possibility in M3D of reading initial equilibria in EQDSK format, which is a standard input for many numerical codes and also a normal way of storing experimental equilibria data.

After reading the equilibrium from the EQDSK, the meshing is then made within the M3D code once the separatrix and the first wall positions are known. The plasma equilibrium from the EQDSK is used to initialize the 3D code at $t = 0$ and then the time evolution begins. Linearly, M3D runs an initial value computation and the growth rate is approximately determined after a few hundred Alfvén times.

In figures 1(a) and (b) the initial mesh for the ITER-AS (advanced scenario) case and the q profile are shown, respectively.

This equilibrium was used first to find the no-wall and ideal wall stability beta limits using the CHEASE (equilibrium preprocessing) [7] and MARS (stability) codes [8]. The CHEASE code is in fact able to generate a series of similar equilibria at different beta's starting from an initial case with a given beta value. The $n = 1$ no-wall stability limit was determined by considering an ideal wall far away from the plasma, while the ideal wall limit was found assuming an ideal wall at a radial position normalized to the plasma minor radius of about 1.3.

Afterwards the M3D code was initialized using the same equilibria and the no wall and ideal wall stability limits have been reasonably reproduced (see figure 2).

We note that to run M3D with two walls, in order to reproduce the ideal wall stability limit, non-trivial modifications of the code have been necessary, since in this case all the velocities have to be set to zero outside the first wall. The agreement between the two codes is reasonably good, considering that they use completely different numerical schemes, for example, MARS is spectral in the poloidal angle, while M3D uses finite elements.

3. M3D nonlinear runs

In the following sections simulations of the fully nonlinear evolution of VDEs are described. Two classes of initial equilibria are considered: analytically obtained elliptical equilibria and EQDSK type equilibria of diverted type configurations (similar to the one presented in section 2).

Generally this second type requires a higher numerical resolution (and consequently longer computational times) due to the complex geometry near the X-point. Although, due to the limited available numerical resources, we have not performed extended convergence studies, the qualitative observation is that high resolution and good meshing near the X-point are really needed for these computations. Another important point to note is that for each of these disruption computations there

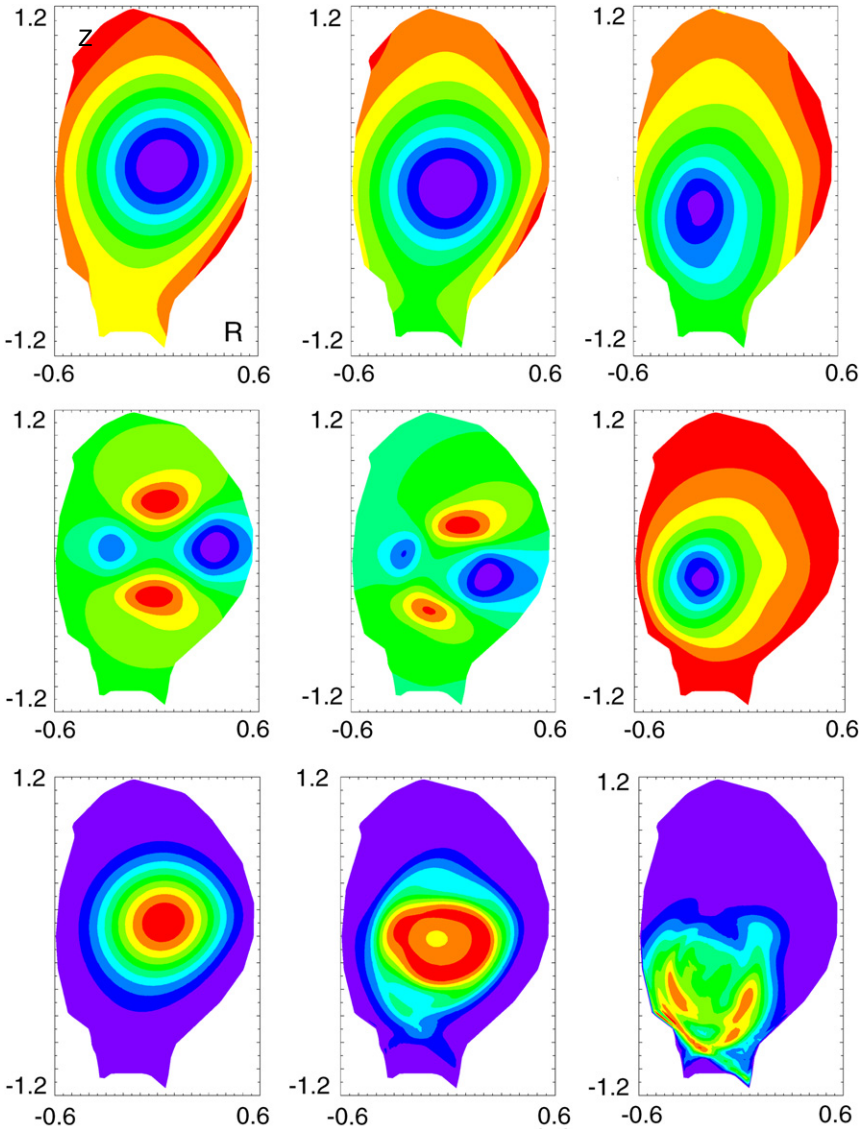

Figure 6. Equilibrium poloidal flux (first row), perturbed poloidal flux (second row) and Temperature (third row) at three different times.

is a final stage of the simulation, to be evaluated case by case, where numerical convergence and resolution are lost, due to the appearance of localized structures in magnetic field, current, velocity and/or pressure.

Where not explicit mentioned differently, values of the Lundquist number (S) (inverse resistivity in our units) and Prandtl number (P) (ratio of viscosity over resistivity) of 10^4 and 10, respectively, are chosen for the cases analysed in the paper.

3.1. Elliptical equilibria

The M3D code has been modified to include the possibility of calculating the initial equilibrium analytically with a simple elliptical (and eventually triangular) shape. The q profile can also be chosen using analytical formulae and specifying the on-axis q.

These elongated equilibria are unstable with a resistive wall even without any non-axi-symmetric perturbation. In figure 3 an example of a 2D simulation of a VDE is shown by plotting the poloidal flux contours at three consecutive times.

In figure 4 the time traces of several average quantities are given: note that the rapid decay of the current and increase in the vertical displacement happens in around $100\tau_A$, which is of the order of the chosen penetration time of the wall (if not explicitly differently mentioned, it has been fixed to this value throughout the paper). For the selected S value this might correspond in physical units to a time in the milliseconds range. Furthermore, from figure 4, a peculiar behaviour of the poloidal beta can be observed, which first increases and then suddenly decreases. This behaviour is due to the initial decrease in the current with an almost constant plasma pressure, while the rapid decreasing phase of the poloidal beta is due to the following loss of the plasma internal energy (thermal quench) not compensated by the simultaneous decrease in the current. The thermal quench happens in the time interval $460\tau_A < t < 520\tau_A$ when the on-axis pressure decreases to 1/10 of its initial value.

If we compare this axi-symmetric ($n = 0$) run, with a similar run where non-axi-symmetric modes with toroidal

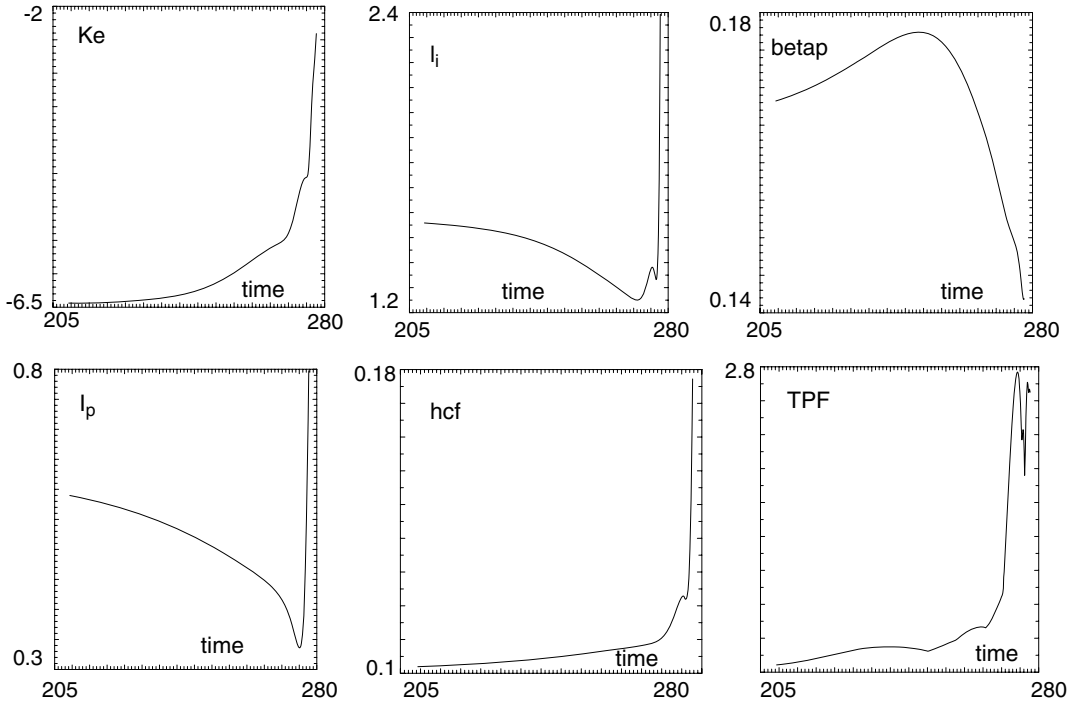

Figure 7. Time traces of perturbed Ke, internal inductance (l_i), poloidal beta (betap), toroidal current (I_p), halo fraction (hcf) and TPF.

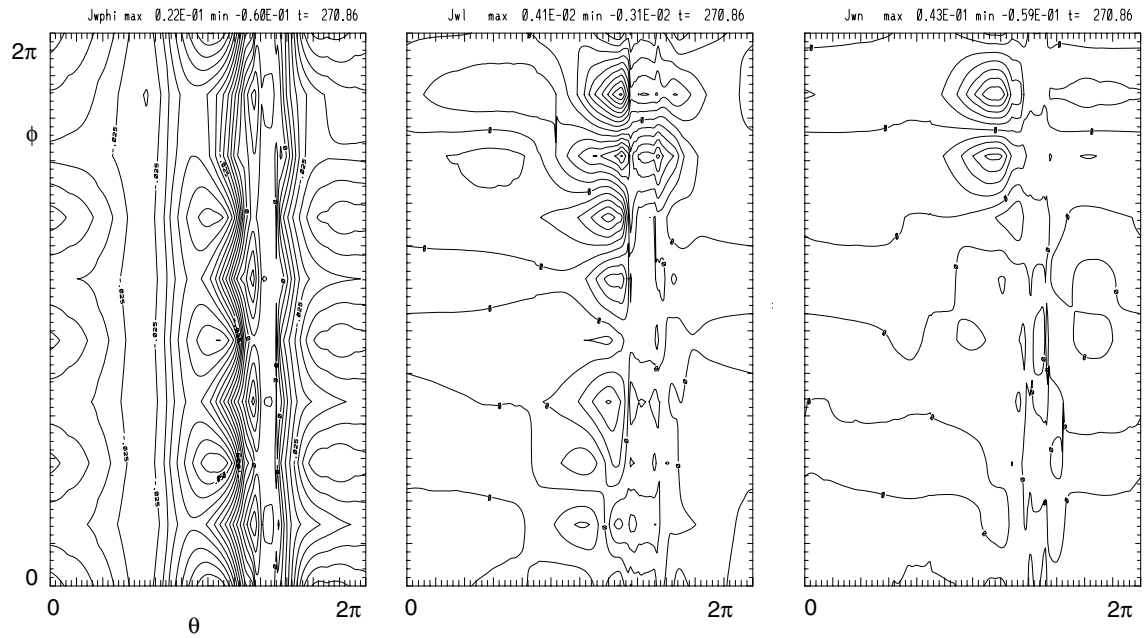

Figure 8. Toroidal, poloidal and normal current components at the wall vs poloidal angle.

mode numbers n up to 4 have been considered, it is seen that the VDE is evolving faster in time (about a factor of 2) with respect to the symmetric case. This confirms already obtained results [1, 9]. However, the toroidal peaking factor (TPF) for this simulation is still around 1 (as in the 2D case), showing that the effect of the non-axi-symmetric perturbation is not big enough. For these cases the $q(0)$ has been initially set slightly above 1. We tried to vary it leaving all the rest identical, in order to see the effect of a destabilization of the 1/1 kink. The main effect is that in the lower $q(0)$ cases, the numerical convergence becomes critical, before a clear VDE could develop. Therefore, we concentrate on the case with $q(0)$ around 1–1.1, which is numerically more stable, and we try to vary the resistivity (and therefore the penetration time) of the wall in order to find a combination of the parameters able to show a clear 2D VDE with a superimposed and also clear and well resolved non-axi-symmetric mode. However, we did not find cases where a clear VDE was accompanied by a TPF appreciably above 1. A simple explanation for this behaviour is that the external kink is stable for these cases, so

that the resistive wall has no effect on the non-axi-symmetric modes.

There are a few important points that we learned from these simulations: we verified that elongated equilibria are, as expected in toroidal geometry, unstable in axi-symmetry (for $n = 0$); secondly, we observed that if $q(0)$ is less than 1 numerical stability is difficult due to the developing of a strongly unstable internal 1/1 kink; finally, we find that the TPF is almost 1 for these mildly unstable cases, where the $n > 0$ part of the spectrum is marginally stable. However, we expect that this will certainly not be the case for the high beta advanced tokamak scenarios.

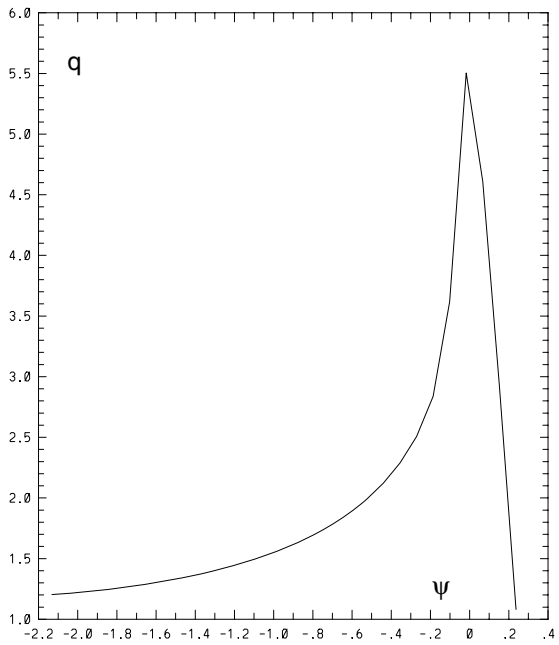

Figure 9. q profile vs poloidal flux for the ITER reference case.

3.2. Diverted tokamak equilibria

By using the ability of reading EQDSK files we initialize the M3D code with realistic diverted equilibria. We consider three different cases, an ASDEX-like equilibrium (that we have already used in previous simulations [9]), an ITER-reference scenario and the ITER-AS case discussed in section 1 for the linear stability benchmark.

3.3. ASDEX-like case

The initial equilibrium is shown in figure 5, it was obtained from an EQDSK file and the on-axis pressure was multiplied by a factor of 3 in order to hit the stability threshold of the external kink.

Contours for three time slices during the VDE of the equilibrium poloidal flux (first row), perturbed poloidal flux (second row) and temperature (third row) are shown in figure 6.

It can be seen that the structure of the perturbed flux is changing in time, from the initial imposed perturbation (left panel, second row) to the final stage, when the plasma is hitting the down-high field side of the wall.

Also the temperature structure is changing a lot during the dynamical evolution showing fine filamentary structures at the end (last row, right panel). Analysing the spectrum of the perturbed field, we observe that $n = 1$ is the dominant part but a lower amplitude $n = 2$ component is also present (n up to 4 should be resolved in this simulation since eight toroidal mesh points have been taken).

In figure 7 the time evolution of macroscopic quantities, including the TPF and the halo current fraction (hcf), is shown. The total plasma current for this case is of about 800 kA. Qualitatively, the time behaviour is similar to that obtained for the simple elliptical case. However, there are important quantitative differences. First of all, the time scale is faster. In around $60\tau_A$ half of the initial current is lost, whereas half of the pressure is lost in the time interval $240\tau_A < t < 270\tau_A$.

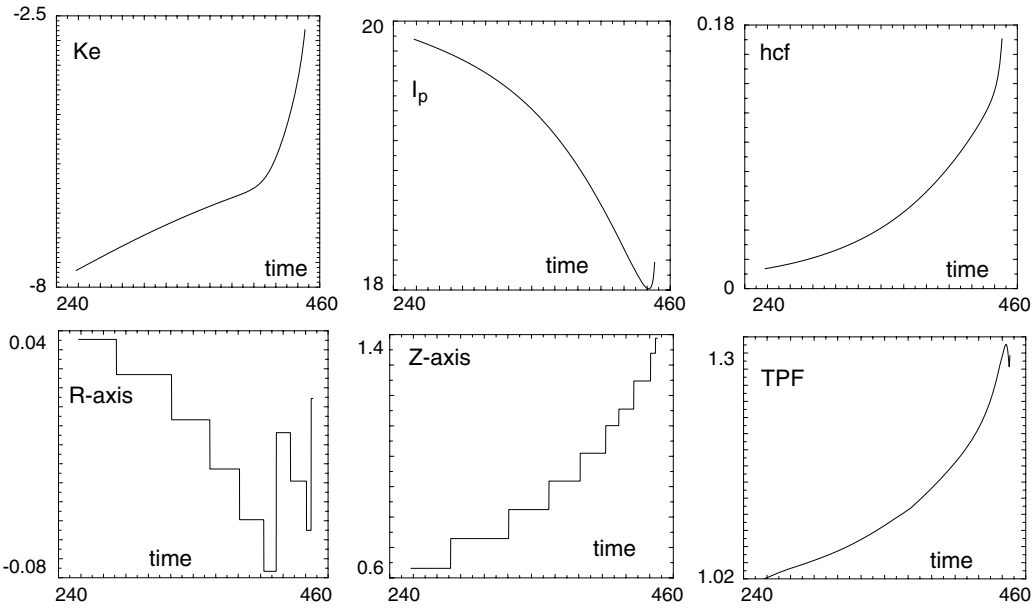

Figure 10. Time traces of Ke, plasma current (I_p), halo fraction (hcf), radial and vertical positions of the magnetic axis (x-axis, y-axis), and TPF.

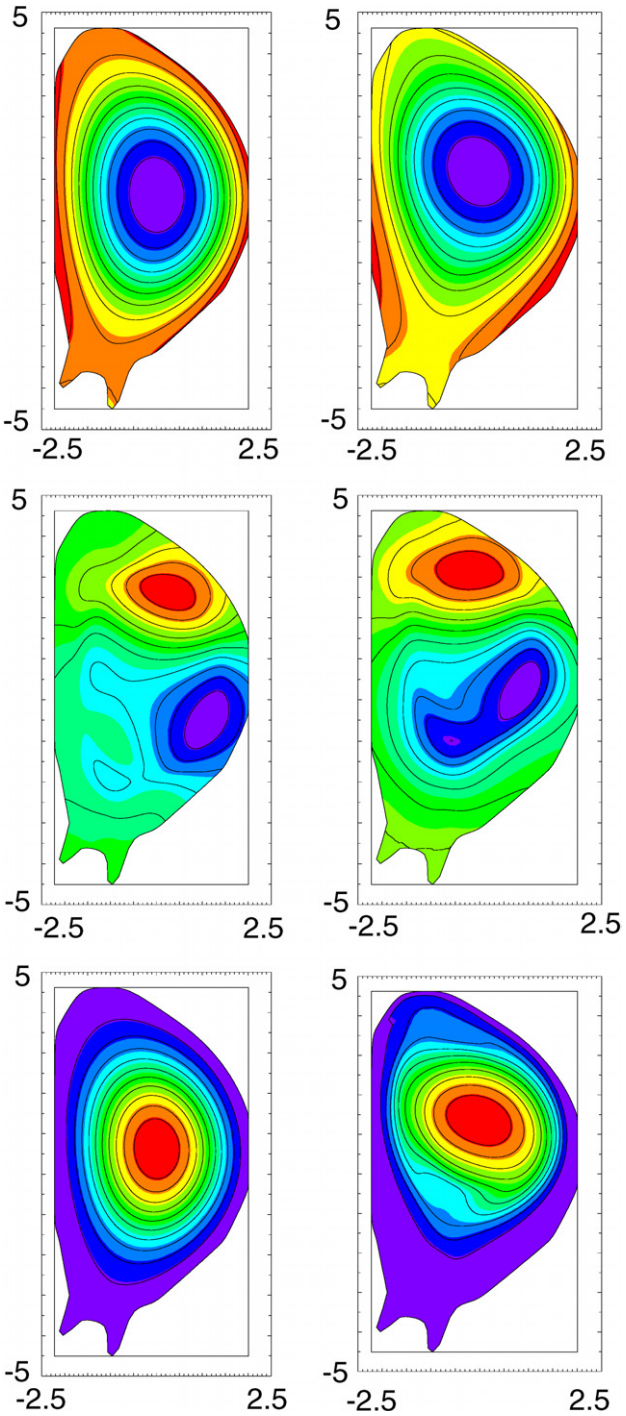

Figure 11. Equilibrium and perturbed poloidal flux (first and second row), temperature third row.

The faster time scale is due to the dominant $n = 1$ external kink activity.

It is also seen that in the last few time steps the TPF grows to a high value. Although at the very end of the simulation ($t > 275\tau_A$) there is a lack of numerical convergence (see the current trace that suddenly increases in time) due to insufficient resolution in this final phase, when strongly localized filamentary structures tend to develop. By considering as 'reliable' the evolution up to $t = 275\tau_A$ it can be seen, from figure 7, that the hcf rises up to 5% while the TPF increases to 2.5–2.6. These values agree with previous estimates [9].

In figure 8 the structure of the current density pattern at the wall at $t = 271\tau_A$ is shown. The vertical axis is the toroidal angle while the horizontal axis is the length in the poloidal plane on the constant flux contour (0 is the low field side of the torus). The first frame is the toroidal current component (Jwphi), the second the tangential (along the constant flux lines, Jwl) while the third frame is the normal component (Jwn). It can be seen that the dominant component on Jwl and Jwn is an $n = 1$ mode, while the current localization is on the inboard side of the torus, as can be expected from the VDE plasma contours evolution plotted in figure 6.

A very important point is to check how these results scale with the plasma resistivity (or the Lundquist number S). As mentioned, these simulations have $S = 10^4$, which is clearly quite unrealistic for normal tokamak operation and even more unrealistic in view of ITER. Unfortunately realistic simulations at S values of the order of 10^8 or 10^9 are completely out of the discussion, due to the prohibitive memory and computer time resources needed. Due to our limited computer resources, we could only check our results by a modest scaling of S up to 10^5. It is, however, interesting to note that, even for such a modest increase, the code ran three times slower and the run lasted for several days. Although qualitatively the VDE followed the same pattern as for the lower S case, there is an important difference in the achieved values of hcf and TPF. In particular, hcf rises again up to 5% but TPF hardly reaches 1.1, i.e. the VDE becomes much more symmetrical. A possible explanation for this is that the growth time of the external kink scales with S. In fact there are no reasons, for values of β below the ideal wall limit, why the external kink should not scale with plasma resistivity. We verified, by comparing the two cases, that the lowest S has the higher perturbation at the wall during the final stage of the VDE (even in the presence of a slower evolution of the high S case, as expected due to the higher global resistive diffusion time).

From these considerations, it appears clear that there are two competing mechanisms during the VDE: on the one hand the plasma β which enhances the instability of the external ideal kink, and on the other hand the effect of a higher resistivity (i.e. lower temperature) that can induce a faster evolution of the resistive kink.

In real experimental high S, high β cases, possibly the predominant effect will be that of the nonlinear evolution of the ideal kink instability. Therefore, it can be expected that when the current quench precedes the thermal quench (normal VDE), the high β discharge can produce a relatively high TPF; however, since the current was already partially lost (due to the vertical displacement which 'scrape-off' the plasma current), the hcf is not expected to be particularly high. In contrast, in cases when the thermal quench happens first (standard disruption), it can be expected that the degree of asymmetry becomes lower (since the external, and possibly also the internal, kinks are mitigated) but the hcf can be relatively higher due to the high current still flowing in the plasma. This qualitative trend is in agreement with the empirical hyperbolic law, (TPF$\times$hcf) $<$ const, found in experiments [1]. The apparently contradictory fact that '*events starting with a thermal collapse usually have much smaller halo fraction and*

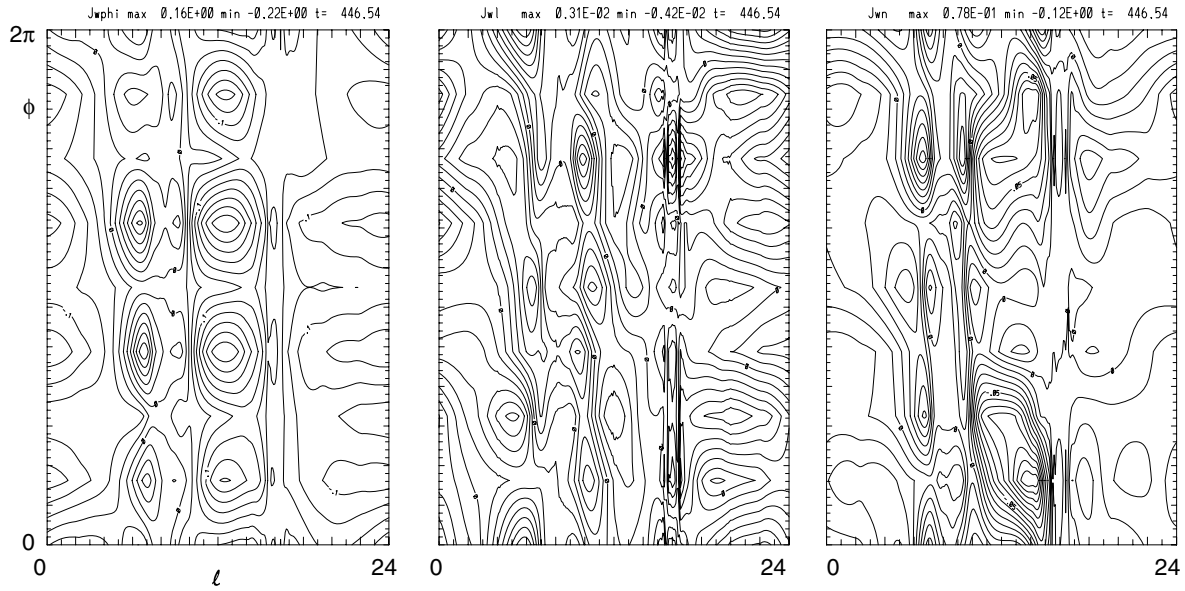

Figure 12. Toroidal, poloidal and normal current components at the wall vs poloidal length.

hardly any asymmetry' [1] has been interpreted in terms of the q at the edge, which is believed to remain higher (above 1.5) in these cases and therefore to enhance plasma stability. In our simulations, however, the pressure seems to be the leading stabilization/destabilization cause for the external kink not the q behaviour. The main point here is that the plasma should evolve towards an external kink unstable configuration for the TPF to become high.

However, as mentioned, we have not looked at cases with $q(0) < 1$, where the internal kink can play a role and for which the current reconnection effects and q profile fast changes during the disruption can be dominant.

3.4. ITER-reference scenario

This ITER-reference scenario shows many similarities to the previous Asdex-like case. The initial q profile is given in figure 9; it is of the order of 1.2 in the centre.

The nonlinear evolution shows a clear upward-inward VDE as shown by the average quantities time evolution in figure 10. The TPF and hcf rise up to 1.3 and 15% of the equilibrium current, respectively, i.e. around 2.2 MA since the reference ITER scenario has around 15 MA of total plasma current. Note that the hcf percentage is much higher if compared with the ASDEX case, but (TPF $\times$ hcf) product is still fully compatible with the experimental results [1]. Another thing that can be noted from figure 10 is that the Ke increase has clearly two distinct phases, an initial slower and a second faster one, which is very likely due to the external kink nonlinear development.

The flux contours of the equilibrium and perturbed magnetic fluxes (first and second rows) and of the temperature (third row) are shown in figure 11, at the initial and final phases of the VDE.

The well-defined temperature contours clearly show that the thermal quench has not occurred yet, and, as noted before, this is consistent with a relatively high TPF and hcf. In fact, in the time interval $200\tau_A < t < 440\tau_A$ the plasma pressure changed by no more than 30%.

Finally in figure 12 the halo current components (toroidal, tangential and normal) are shown in the toroidal–poloidal plane at the wall. Again the current pattern is described predominately by an $n = 1$ concentrated at the poloidal angle where the VDE is pushing the plasma (upwards in this case).

3.5. ITER-AS case

This case has also been obtained by an EQDSK file and the mesh and q profile are given in figure 1. In this section we look at the nonlinear evolution of this reversed shear ITER equilibrium choosing a normalized beta of 3.5.

We note that the initial equilibrium is almost touching the outboard side of the wall. A more realistic simulation will probably require a double wall calculation, since in ITER, the blanket modules, which face the plasma, do not correspond to the actual stabilizing shell (as instead is the case here).

In figure 13 the (Z, R) contour plots for the average poloidal flux (first row), perturbed magnetic field potential (second row) and temperature (third row) are shown at the initial (left frame) and final stages (right frame) of the simulation. It is seen that, for similar plasma and wall physical parameters, the up–down movement is slower in this case with respect to the ASDEX case (figure 6) or to the ITER-reference case (figure 11). In almost twice the time of the ASDEX case, the plasma centroid has moved much less in the vertical direction. This conclusion of a relatively stronger vertical stability of the reversed shear equilibrium was already observed in 2D plasma simulations [10]. It can be argued that a stronger coupling exists between the reversed shear displaced plasma current and the passive structures.

On the other hand, in this case while the TPF rises up to 1.2–1.3 the hcf is about 30% of the mean plasma current, i.e. much higher than the previous cases. This is also not surprising since much of the equilibrium current density is concentrated, for this ITER-AS case, near the wall.

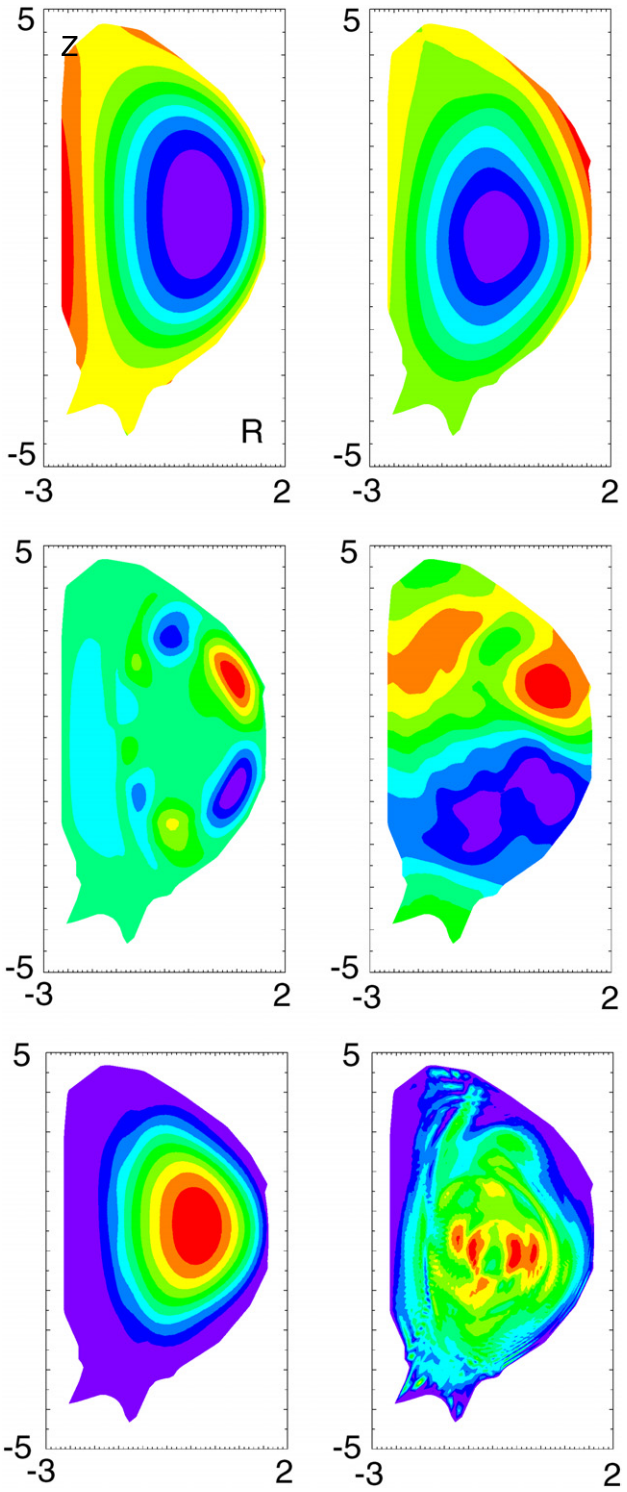

Figure 13. Equilibrium and perturbed poloidal flux (first and second rows), temperature third row.

In figure 14 the current density components (toroidal, tangential and normal) at the wall are shown.

The current structure is more complicated than in the ASDEX-like case (see figure 8), with the presence of higher order modes even in the poloidal and normal current components. We note that for this simulation the dominant toroidal harmonic is the $n = 2$ mode (harmonics up to $n = 4$ should be resolved by the toroidal mesh) with the presence also of a slightly lower $n = 1$ subdominant mode.

We tried to increase also in this case the Lundquist number to $S = 10^5$. Obviously, the simulation time increased quite a bit and we were not able to clearly show the VDE, since the numerical resolution becomes critical near the wall for some quantities, especially the perturbed toroidal field (see figure 15) and perturbed current, which tend to become increasingly concentrated near the wall. Therefore, this simulation could not be considered satisfactory from the point of view of the numerical convergence.

Nevertheless, since the other quantities are perfectly well behaving, it may be useful to observe that in this case the TPF increases to 1.6–1.7 while hcf remains low (<3.5%), again in agreement with the experimentally observed hyperbolic trend. The long simulation time due to the relatively high S value, the already observed resilience of the reversed shear configuration to the 2D vertical displacement and finally the high instability of the external kink due to the relatively high beta produce an increase in the non-axi-symmetric perturbation amplitude, and therefore of the TPF, but leaving the hcf very low, since the equilibrium current is almost not displaced from its initial distribution during this evolution. For example, when compared with the ITER-reference scenario, the flux contours have moved downwards less than half the distance that can be evaluated from figure 11 (upper panel), in a similar time interval.

4. Discussion and conclusions

A big effort has been made to numerically simulate VDEs and disruptions in tokamaks by employing an MHD code which is able to deal with realistic geometry, diverted plasmas and with non-ideal boundary conditions, i.e. a resistive shell through which the magnetic field can penetrate in time.

To our knowledge, these are the first simulations of VDEs' induced disruptions, which include the contribution of non-axi-symmetric modes, in particular, the external kink.

We have seen that these simulations can effectively help to understand several qualitative features of the plasma dynamics during the VDEs.

These simulations are in qualitative agreement with experimental results obtained so far.

For example, we add the results of our simulations on the TPF versus halo fraction plot published in [1] (and reproduced here in figure 16) finding satisfactory agreement.

We think that this paper contributes to a clarification of the competing effects of the thermal collapse and high TPFs for external kink dominated VDEs. It shows that with a homogeneous wall, the halo current tends to concentrate poloidally near the region where the plasma touches the material wall having a toroidal structure which is mainly $n = 1$, but which can also become more localized ($n > 1$) in advanced scenarios. In this case a stabilizing role of the 'natural' high halo fraction, which can develop due to equilibrium current peaking near the separatrix region, in AS cases for ITER has been found and as a consequence of the enhanced current to the wall the slowing down of the VDEs. It remains an open question whether in this kind of configurations, the high hcf could also be accompanied by a high TPF. According to the

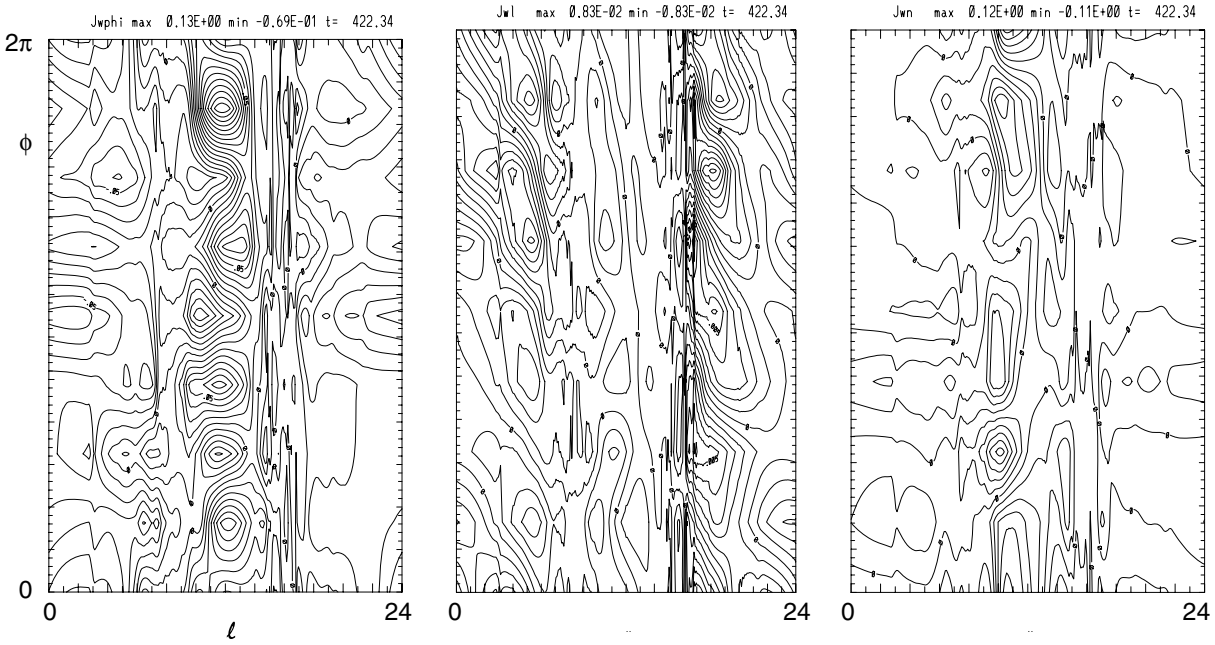

Figure 14. Toroidal, poloidal and normal current components at the wall vs poloidal length.

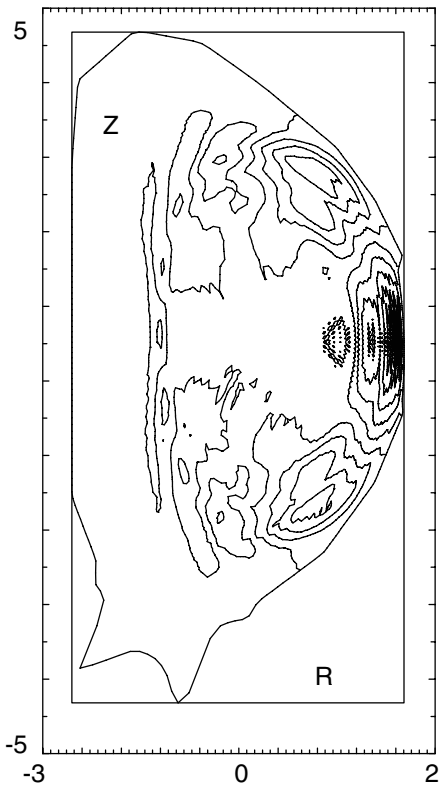

Figure 15. Perturbed toroidal field.

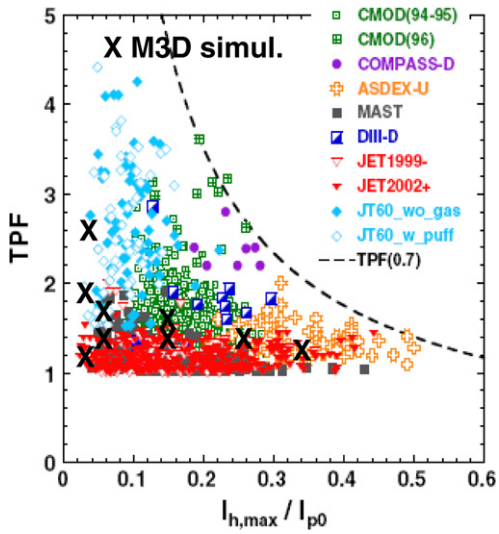

Figure 16. TPF versus halo current fraction (hcf) (figure modified from [1]).

simulations presented here, it may be that the 'hyperbolic law' is also true for plasma in advanced scenarios. In fact, we have obtained a case at higher TPF in which the hcf was relatively small. This case has shown, however, as discussed above, an unsatisfactory numerical convergence in the final phase. An interesting point, to be perhaps addressed experimentally in real devices, is also the presence of higher order toroidal modes ($n = 2$) in AS cases.

Several things need to be improved in future simulation work. In particular, the role of the externally applied vertical field during the VDE is not studied in this paper, where the externally applied currents are supposed to be frozen (at the initial time) during the plasma evolution. The numerical convergence during the development of internal MHD modes, especially when $q(0) < 1$, also needs to be addressed. Moreover, higher resolution runs are mandatory in all cases but especially in advanced scenarios. This is clearly a question about the available computational resources and the degree of parallelization. All the simulations presented here are done using the OpenMP parallel version of M3D, which distributes

each toroidal mesh point calculation to different processors in shared memory machines. New simulations using the massive parallel MPI version of the code are planned for the near future. These simulations will also hopefully permit higher Lundquist numbers runs (S up to 10^6 or 10^7) which are needed to understand the scaling laws of the relevant modes. Finally the effect of the heat transport and of different heat transport models should possibly be better clarified, since we have clearly shown that the thermal quench can largely influence us, on the other hand, is also often observed in experiments, the modes evolution, toroidal peaking factor and halo current.

Acknowledgments

The authors kindly acknowledge A. Pletzer for the development of the GRIN solver. R.P. thanks Mario Cavinato for providing the ITER equilibria and S. Ortolani, G. Pautasso and V. Riccardo for very helpful discussions. This study was partially carried out under EFDA Contract No 05-1335.

References

[1] Hender T. *et al* 2007 MHD stability, operational limits and disruptions (chapter 3) *Nucl. Fusion* **47** S128–202
[2] Pomphrey N., Bialek J.M. and Park W. 1998 *Nucl. Fusion* **38** 449
[3] Park W., Belova E.V., Fu G.Y., Tang X.Z., Strauss H.R. and Sugiyama L.E. 1999 *Phys. Plasmas* **6** 1796
[4] Strauss H.R. and Longcope W. 1998 *J. Comput. Phys.* **147** 318–36
[5] Strauss H. 2004 *Comput. Phys. Commun.* **164** 40
[6] Chance M. 1997 *Phys. Plasmas* **4** 2161
[7] Lutjens H., Bondeson A. and Sauter O. 1996 *Comput. Phys. Commun.* **97** 219
[8] Bondeson A. *et al* 1992 *Phys. Fluids* B **4** 1889
[9] Paccagnella R. *et al* 2005 Vertical diplacement events simulations for tokamak plasmas *Fusion Eng. Des.* **75** 589
[10] Beghi A. *et al* 2001 *Fusion Eng. Des.* **56–57** 777